

The effect of the cathode tip angle on the GTAW arc and weld pool: I. Mathematical model of the arc

This article has been downloaded from IOPscience. Please scroll down to see the full text article.

1997 J. Phys. D: Appl. Phys. 30 2744

(<http://iopscience.iop.org/0022-3727/30/19/013>)

View [the table of contents for this issue](#), or go to the [journal homepage](#) for more

Download details:

IP Address: 128.233.210.97

The article was downloaded on 05/05/2013 at 10:46

Please note that [terms and conditions apply](#).

The effect of the cathode tip angle on the GTAW arc and weld pool: I. Mathematical model of the arc

Massoud Goodarzi[†], Roland Choo[‡] and James M Toguri

Department of Metallurgy and Materials Science, University of Toronto, Toronto, ON M5S 3E4 Canada

Received 10 February 1997, in final form 26 June 1997

Abstract. By developing mathematical models for the arc and the weld pool in the GTAW process, the effect of the electrode tip angle on both arc and weld pool was studied. The present paper is concerned with the model for the arc. By applying a variable cathode surface area, the effect of the electrode tip angle (in the range of 10 to 150°) on the arc properties, especially on the anode current density, heat flux and gas shear stress over the weld pool, was investigated. Comparison of the calculated results with the available experimental data for 200 A arcs of different lengths showed that the model predictions for temperatures higher than 10 000 K are in very good agreement. For temperatures less than 10 000 K, some modifications were necessary to take into account the absorption of heat by the cooler parts of the arc. It was found that by increasing the electrode tip angle, the anode spot at the weld pool surface tended to be more localized. This led to a higher maximum heat flux and anode current density. On the other hand, the gas shear stress increased on decreasing the electrode tip angle.

Nomenclature

B_θ	Azimuthal component of magnetic field (T)	h	Enthalpy (J kg ⁻¹)
C_p	Specific heat at constant pressure (J kg ⁻¹ K ⁻¹)	h_e	Enthalpy of the gas at T_e (J kg ⁻¹)
\mathbf{J}	Current density vector (A m ⁻²)	h_w	Enthalpy of the gas at T_w (J kg ⁻¹)
J_a	Anode current density (A m ⁻²)	k	Thermal conductivity (W m ⁻¹ K ⁻¹)
J_C	Cathode current density (A m ⁻²)	k_B	Boltzmann constant (1.38 × 10 ⁻²³ J K ⁻¹)
J_r	Radial current density (A m ⁻²)	q_a	Total anode heat flux (W m ⁻²)
J_z	Axial current density (A m ⁻²)	q_c	Anode heat flux due to convection and conduction (W m ⁻²)
L_{arc}	Arc length (m)	q_e	Anode heat flux due to electrons (W m ⁻²)
P	Pressure (Pa)	q_r	Anode heat flux due to radiation (W m ⁻²)
Pr_w	Prandtl number at T_w	$q_{r,i}$	Radiative heat flux receive by S_i (W m ⁻²)
Q_{ioniz}	Volumetric heat source from the cathode fall to ionize the plasma (J m ⁻³)	r	Radial coordinate, radial distance (m)
R_{elec}	Electrode radius (m)	$r_{i,j}$	Distance between S_i and V_j (m)
S_C	Cathode surface area (m ²)	r_r	Radius of V_j (m)
$S_{R,j}$	Radiation energy source of V_j (J)	r_s	Radius of S_i (m)
S_R	Radiation loss V_j (J s ⁻¹ m ⁻³)	u	Axial velocity (m s ⁻¹)
S_Φ	Source rate of Φ	v	Velocity vector (m s ⁻¹)
T	Temperature (K)	v	Radial velocity (m s ⁻¹)
T_e	Electron temperature at the edge of the plasma (K)	z	Axial coordinate, axial distance (m)
T_w	Temperature of wall (K)	Γ_Φ	Diffusion coefficient of Φ
V_C	Cathode fall voltage (V)	Φ	General conserved property
V_j	The plasma volume element (m ³)	Ψ	The angle that $r_{i,j}$ makes with the normal to S_i (rad)
e	Elementary charge (1.602 × 10 ⁻¹⁹ C)	α	Electrode tip angle (deg)
		ϕ	Electric potential (V)
		ϕ_a	Work function of the anode material (V)
		ϕ_d	Thermal diffusion coefficient of the electron (m ² s ⁻¹)

[†] Present address: Department of Metallurgy & Materials Science, Iran University of Science and Technology, Narmak, Tehran 16844, IR Iran.

[‡] Present address: MBF-PEUGEOT Sdn Bhd, Nos 11 & 15, 2 1/2 Miles, Jalan 4/93, Taman Miharja, 55200 Cheras, Kuala Lumpur, Malaysia.

μ	Newtonian viscosity ($\text{kg m}^{-1} \text{s}^{-1}$)
μ_e	Viscosity of the gas at T_e ($\text{kg m}^{-1} \text{s}^{-1}$)
μ_w	Viscosity of the gas at T_w ($\text{kg m}^{-1} \text{s}^{-1}$)
μ_0	Permeability of free space ($4\pi \times 10^{-7} \text{ N A}^{-2}$)
ζ	Dummy function (m)
ρ	Fluid density (kg m^{-3})
ρ_e	Gas density at T_e (kg m^{-3})
ρ_w	Gas density at T_w (kg m^{-3})
σ	Electrical conductivity ($\Omega^{-1} \text{ m}^{-1}$)
τ	Shear stress (N m^{-2})

1. Introduction

The welding of metal components is a major part of many manufacturing processes and the integrity and soundness of the final product depend on the strength of the weldment. The quality of welds, on the other hand, is determined by metallurgical changes in the weldment, including the fusion zone and the heat-affected zone, and the geometry of the weld pool. It has been shown that the puddle geometry, the temperature gradients, the local cooling rates and the solidification structure can be significantly influenced by heat and fluid flows into the weld pool [1]. The geometry of the weld pool, in gas tungsten arc welding (GTAW) specifically, can change with variation in the shape of the electrode tip [2]. In addition, other weld characteristics, such as weld penetration, surface smoothness, segregation pattern and gas porosity, can be affected by changes in the flow pattern in the weld pool [3]. In the case of the arc welding processes, the heat and fluid flows in the weld pool are determined by the electromagnetic force, the buoyancy, the surface tension [4], and the impinging force of the arc plasma [5]. Gas shear stress also can be a parameter affecting the flow pattern into the weld pool, especially for high-current arcs [6].

The description of the input energy and the electric current sources are basic to every numerical model simulating a weld, and the resultant output is affected by these two sources. There are many numerical models described for fluid and heat flows of the weld pool in GTAW [4, 5, 7–13]. In the majority of these models, the heat flux and electric current density from the arc are defined to have a Gaussian distribution at the top of the weld pool.

In the available models for the welding arc [14–26], there has been no attempt to quantify either the heat flux and the electric current density distribution at the top of the weld pool, or the effect of the electrode tip angle on these properties. This paper is concerned with a mathematical model for the welding arc with a tapered electrode. A second paper on the effect of the electrode tip angle on the weld pool geometry is presented separately.

2. Model description

Figure 1 shows a schematic diagram of a direct current electrode negative (DCEN) gas tungsten welding arc. A voltage difference between the electrodes produces an

electric current in the space between the electrodes if the gas in this space is ionized. Thermally emitted electrons from the cathode (tungsten electrode) strike the neutral atoms in the arc gap and ionize them and finally condense on the surface of the anode. The passage of the electrons between the cathode and the anode (workpiece) produces a magnetic field. In the arc region of variable cross section, the interaction of the current with its self-induced magnetic field leads to the phenomena of induced plasma jets [27]. Also, the current of electrons through the plasma produces heat through Joule heating, which is sufficiently high to keep the ionized gas stable.

Although a plasma consists of at least three different particles—electrons ions and neutral atoms—it can be treated as a continuum fluid since a high-intensity high-pressure arc is collision dominated [28]. In this case, the equations for the conservation of mass, momentum and energy can be written for the plasma. Together with this fact, the following assumptions which are commonly employed in arc modelling are considered.

(i) It is assumed that the arc is axially symmetric so that the equations can be written in two-dimensional cylindrical coordinates.

(ii) It is assumed that the arc is in a steady state so that the variation of different parameters with time is eliminated.

(iii) It is assumed that the arc is in local thermodynamic equilibrium (LTE) and that the plasma is optically thin.

(iv) Laminar flow is assumed. This assumption was justified by McKelliget and Szekely [29] on the basis of a laminar–turbulent transition for a free jet.

3. Governing equations

Using the above assumptions, the conservation equations can be written as follows.

Conservation of mass.

$$\frac{\partial}{\partial z}(\rho u) + \frac{1}{r} \frac{\partial}{\partial r}(\rho r v) = 0. \quad (1)$$

Conservation of axial momentum.

$$\begin{aligned} \frac{\partial}{\partial z}(\rho u^2) + \frac{1}{r} \frac{\partial}{\partial r}(\rho r v u) = & -\frac{\partial P}{\partial z} + 2 \frac{\partial}{\partial z} \left(\mu \frac{\partial u}{\partial z} \right) \\ & + \frac{1}{r} \frac{\partial}{\partial r} \left[r \mu \left(\frac{\partial u}{\partial r} + \frac{\partial v}{\partial z} \right) \right] + J_r B_\theta. \end{aligned} \quad (2)$$

Conservation of radial momentum.

$$\begin{aligned} \frac{\partial}{\partial z}(\rho v u) + \frac{1}{r} \frac{\partial}{\partial r}(\rho r v^2) = & -\frac{\partial P}{\partial r} + \frac{\partial}{\partial z} \left[\mu \left(\frac{\partial v}{\partial z} + \frac{\partial u}{\partial r} \right) \right] \\ & + \frac{2}{r} \frac{\partial}{\partial r} \left(\mu r \frac{\partial v}{\partial r} \right) - \mu \frac{2v}{r^2} - J_z B_\theta. \end{aligned} \quad (3)$$

The last terms in the momentum equations are due to interaction of the current and its self-induced magnetic field (Lorentz force).

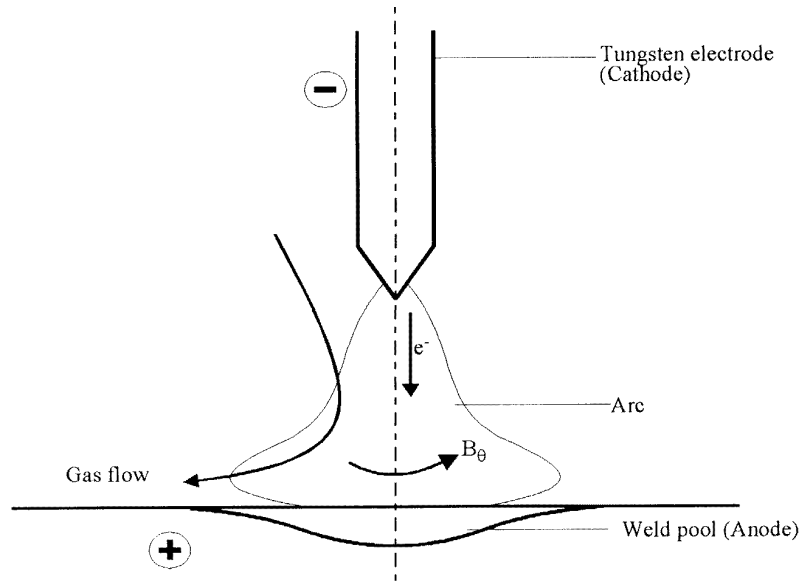


Figure 1. Schematic diagram of the welding arc (GTAW).

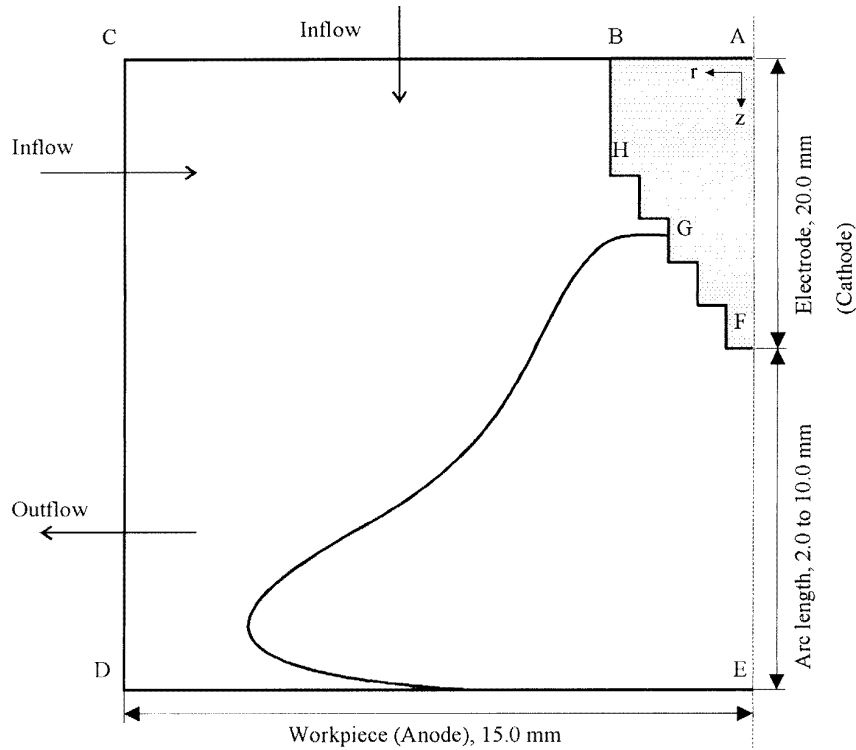


Figure 2. Calculation domain for tapered electrode GTAW (schematic).

Conservation of energy.

$$\frac{\partial}{\partial z}(\rho u h) + \frac{1}{r} \frac{\partial}{\partial r}(\rho r v h) = \frac{\partial}{\partial z} \left(\frac{k}{C_p} \frac{\partial h}{\partial z} \right) + \frac{1}{r} \frac{\partial}{\partial r} \left(\frac{k}{C_p} r \frac{\partial h}{\partial r} \right) + \frac{J_z^2 + J_r^2}{\sigma} - S_R + \frac{5k_B}{2e} \left(J_z \frac{1}{C_p} \frac{\partial h}{\partial z} + J_r \frac{1}{C_p} \frac{\partial h}{\partial r} \right). \quad (4)$$

The source terms in the energy equation are Joule heating, radiation loss and heat transfer due to electron drift.

Continuity of current can be written in terms of the electric potential as:

$$\frac{\partial}{\partial z} \left(\sigma \frac{\partial \phi}{\partial z} \right) + \frac{1}{r} \frac{\partial}{\partial r} \left(\sigma r \frac{\partial \phi}{\partial r} \right) = 0. \quad (5)$$

The azimuthal component of the magnetic field can be

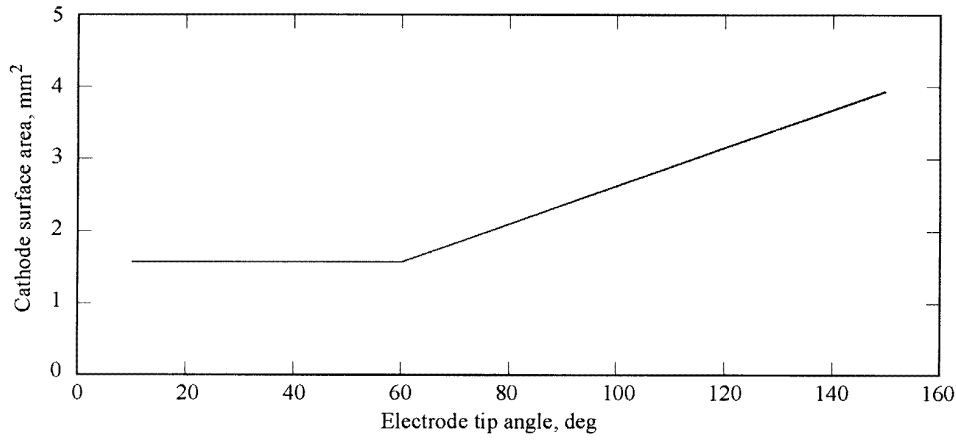


Figure 3. Variation of the cathode surface area with the electrode tip angle.

Table 1. Boundary conditions.

	FG	GH	HB	AB	BC [†]	CD [†]	DE	EF
v	0	0	0	—	0	$\partial v/\partial r = 0$	0	0
u	0	0	0	—	$u = \text{constant}$	$\partial u/\partial r = 0$	0	$\partial u/\partial r = 0$
	$T = 3000 \text{ K}$					Inflow $T = 1000 \text{ K}$	Equation (12)+	
h	$Q_{ioniz} = J_C V_C$	$T = 3000 \text{ K}$	$T = 3000 \text{ K}$	—	$T = 1000 \text{ K}$	Outflow: $\partial h/\partial r = 0$	$J_a \phi_a$	$\partial h/\partial r = 0$
ϕ	$S_C = f(\alpha)$	$J_r = 0$ $J_z = 0$	$J_r = 0$	$J_z = I/\pi R_{elec}^2$	$\partial \phi/\partial z = 0$	$\partial \phi/\partial r = 0$	$\phi = \text{constant}$	$\partial \phi/\partial r = 0$

[†] At these two boundaries, pressure is fixed to a constant value.

Table 2. The corresponding quantities for the different conservation equations.

Equation	Φ	Γ_ϕ	S_Φ
Mass	1	0	0
Axial momentum	u	μ	$-\frac{\partial P}{\partial z} + \frac{\partial}{\partial z} \left(\mu \frac{\partial u}{\partial z} \right) + \frac{1}{r} \frac{\partial}{\partial r} \left(\mu r \frac{\partial v}{\partial z} \right) + J_r B_\theta$
Radial moment	v	μ	$-\frac{\partial P}{\partial r} + \frac{\partial}{\partial z} \left(\mu \frac{\partial u}{\partial r} \right) + \frac{1}{r} \frac{\partial}{\partial r} \left(\mu r \frac{\partial v}{\partial r} \right) - \mu \frac{2v}{r^2} - J_z B_\theta$
Energy	h	k/C_P	$\frac{J_r^2 + J_z^2}{\sigma} - S_R + \frac{5}{2} \frac{k_B}{e} \left(J_z \frac{1}{C_P} \frac{\partial h}{\partial z} + J_r \frac{1}{C_P} \frac{\partial h}{\partial r} \right)$
Electric potential	ϕ	σ	0

calculated from Ampere's law:

$$B_\theta = \frac{\mu_0}{r} \int_0^r J_z \zeta \, d\zeta \quad (6)$$

and the current density can be calculated from Ohm's law:

$$\mathbf{J} = \sigma \nabla \phi. \quad (7)$$

The physical properties of argon, namely density, viscosity, thermal conductivity, heat capacity and electrical conductivity, are treated as a function of temperature and were taken from the tabulated data of Boulos *et al* [30]. The radiation loss data were taken from the work of Evans and Tankin [31].

4. Boundary conditions and numerical method

4.1. Boundary conditions

The calculation domain is shown in figure 2. For all variables, except the electric potential, the calculation domain is BCDEFGH. For the electric potential the tungsten electrode is also added to the calculation domain. A non-uniform grid point system is employed with finer grid sizes near the cathode region. The distance between the electrodes varies from 2.0 to 10.0 mm. The inflow boundary at the top of the domain is taken at 20.0 mm above the tungsten electrode tip. The boundary at the side is 15 mm away from the axis of symmetry. The corresponding boundary conditions are given in table 1.

Table 3. Arc parameters for different arc lengths and electrode tip angles. (T_{max} (K); u_{max} (m s⁻¹); $\Delta\Phi$ (V); ΔP_a (Pa)).

Arc length (mm)	Arc properties	Electrode tip angle (deg)										
		9.18	14.36	20.74	28.36	37.33	47.78	60.00	72.77	100.06	131.41	150.00
2.0	T_{max}	15 760	17 270	18 750	19 850	20 630	21 090	21 510	20 910	18 950	17 940	17 680
	u_{max}	261.1	301.7	339.8	362.6	370.5	364.4	356.7	304.1	191.0	127.6	98.05
	$\Delta\Phi$	7.063	8.175	9.053	9.666	10.08	10.32	10.59	10.35	9.825	9.747	10.02
	ΔP_a	1447	1529	1596	1607	1569	1487	1397	1170	748.4	583.6	515.3
5.0	T_{max}	15 880	17 310	18 670	19 700	20 450	20 950	21 340	20 910	19 110	17 930	17 420
	u_{max}	354.8	387.3	407.2	415.3	414.2	405.9	391.9	353.3	263.1	216.8	190.9
	$\Delta\Phi$	9.072	10.16	11.02	11.64	12.07	12.37	12.68	12.55	12.16	12.12	12.34
	ΔP_a	1390	1496	1534	1519	1466	1387	1278	1102	741.8	593.7	514.4
10.0	T_{max}	15 860	17 290	18 660	19 680	20 380	20 910	21 330	20 720	19 050	17 850	17 440
	u_{max}	354.8	387.0	406.7	413.8	410.1	402.8	389.9	343.4	261.5	216.9	193.6
	$\Delta\Phi$	11.52	12.64	13.52	14.15	14.58	14.91	15.25	15.05	14.74	14.73	14.99
	ΔP_a	952.2	1039	1079	1078	1035	989.6	90.21	749.8	522.9	427.3	371.5

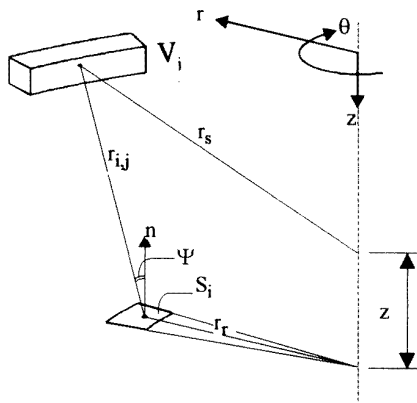


Figure 4. Configuration of radiation view factors.

4.1.1. The cathode region. The conditions for the enthalpy and the electric potential at this boundary are very critical. For the electric potential, it was assumed that the cathode surface area (FG) is a function of the electrode tip angle and the current density distribution on the assigned cathode surface was adjusted so that the total current entering was equal to the applied current. This assumption was made to simulate the real situation in which the current density is not a constant value over the cathode spot surface.

Haidar and Farmer [32] have measured the electrode surface area covered by the plasma for a range of electrode tip angles. From this information, the cathode surface area (the electron emission surface), for angles less than 60° is constant and above 60°, up to 180°, it increases linearly with the electrode tip angle. The cathode surface area for the 60° angle and the slope of the line were determined by comparing the calculated arc temperatures and the experimental data of Haidar and Farmer [32] at 1.5 mm from the tip of the electrode. Variation of the cathode surface area with the electrode tip angle is shown in figure 3.

For the enthalpy, by assuming that the electrons are in a free fall across the cathode sheath, McKelliget and Szekely

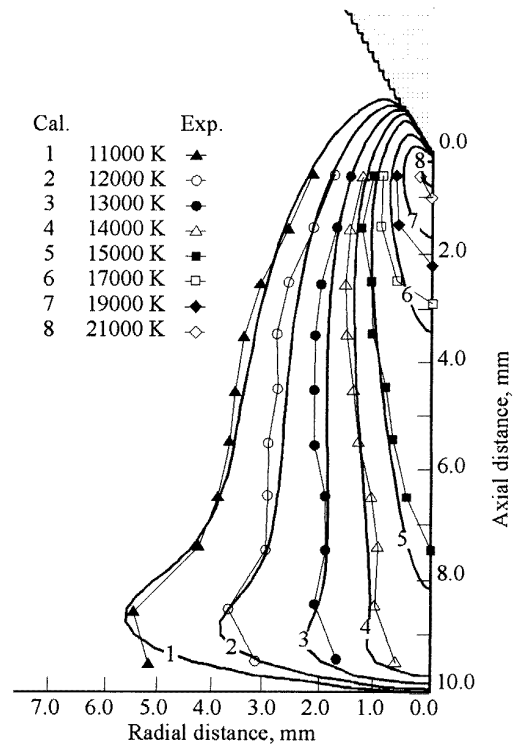


Figure 5. Isotherms of 10.0 mm arc in comparison with the experimental results of Hsu *et al* [14].

[29] presented a model to evaluate the cathode fall voltage, V_C , as follows:

$$V_C = \frac{5 k_B T_e}{2 e} \quad (8)$$

where T_e is the temperature of electrons in the vicinity of the cathode spot. Based on this voltage, a heat source for the arc column can be considered as follows:

$$Q_{ioniz} = |J_C| V_C. \quad (9)$$

It is also assumed that the electrode surface is at a constant temperature close to the melting point of the electrode material. Although the temperature of the cathode surface

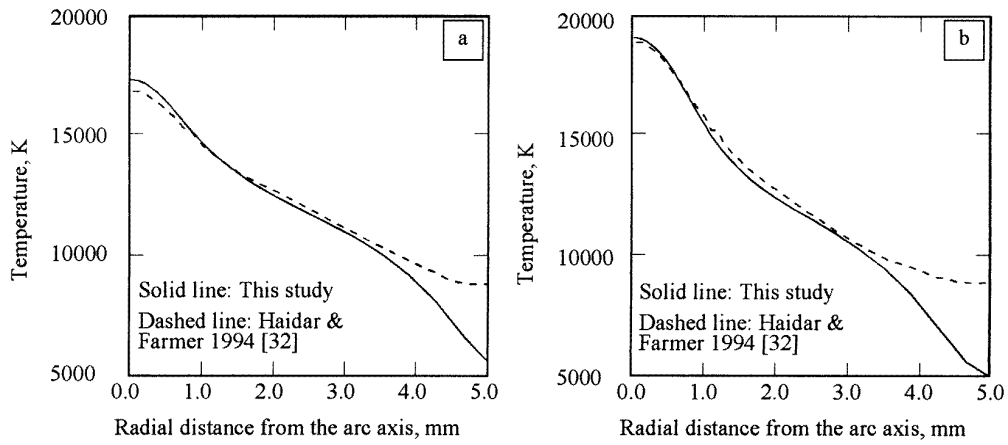


Figure 6. Radial distribution of temperature at 1.5 mm from the cathode tip is compared with the experimental data [32]. $L_{arc} = 5.0$ mm. (a) $\alpha = 20.74^\circ$ (exp.: $\alpha = 18^\circ$); (b) $\alpha = 60^\circ$.

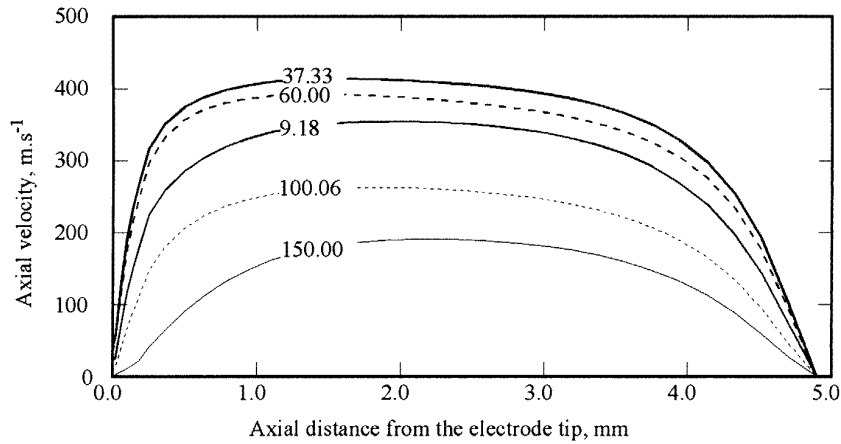


Figure 7. Variation of the axial velocity distribution with electrode tip angle. $L_{arc} = 5.0$ mm. Numbers on the curves are electrode tip angles in degrees.

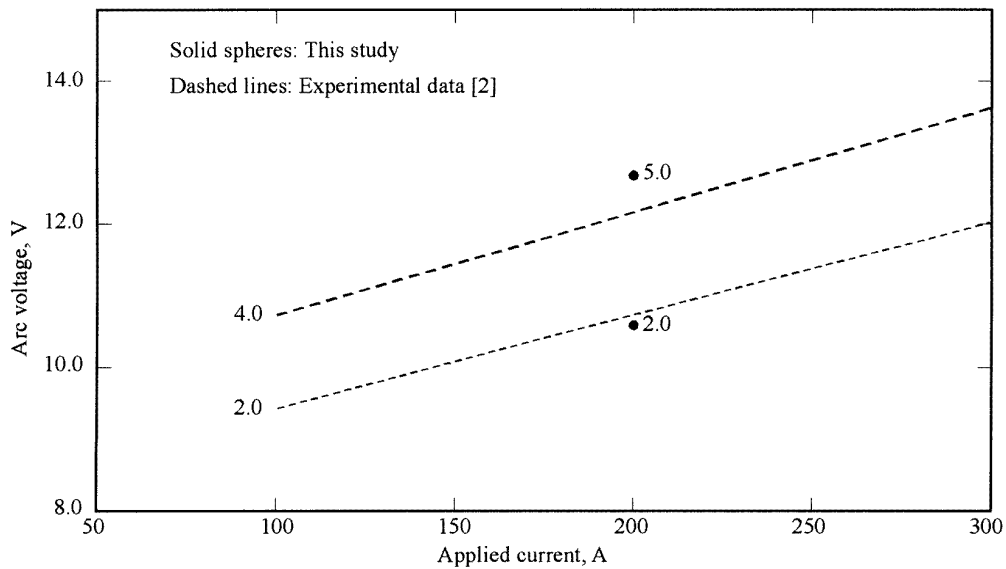


Figure 8. Variation in the arc voltage with arc length in comparison with the experimental data [2]. Numbers are length of arc in millimetres.

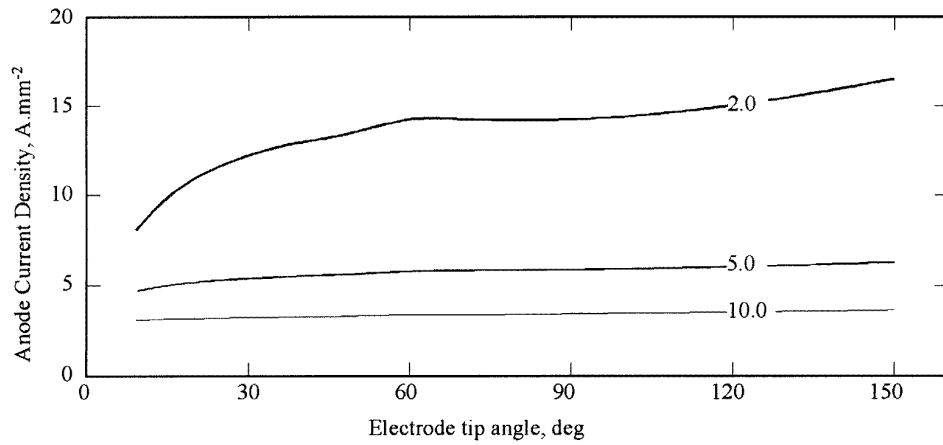


Figure 9. Variation of maximum anode current density with electrode tip angle and arc length. Numbers are arc length in millimetres.

Table 4. Maximum anode current density, maximum anode heat flux and maximum temperature of the gas on the anode surface for different electrode tip angles and arc lengths. ($J_{a,max}$ (A mm⁻²); $q_{a,max}$ (W mm⁻²); $T_{a,max}$ (K)).

Arc length (mm)	Arc properties	Electrode tip angle (deg)											
		9.18	14.36	20.74	28.36	37.33	47.78	60.00	72.77	100.06	131.41	150.00	
2.0	$J_{a,max}$	8.053	9.706	11.06	12.06	12.83	13.40	14.24	14.23	14.39	15.52	16.51	
	$q_{a,max}$	70.42	87.54	102.3	112.7	119.5	123.1	128.4	120.9	106.1	106.4	109.6	
	$T_{a,max}$	12840	13360	13690	13870	13960	13970	13980	13680	12760	12180	11890	
5.0	$J_{a,max}$	4.671	4.966	5.179	5.345	5.478	5.589	5.761	5.795	5.887	6.093	6.260	
	$q_{a,max}$	52.46	60.17	65.36	68.30	69.57	69.60	69.21	64.93	54.73	51.46	49.98	
	$T_{a,max}$	12800	13200	13440	13560	13610	13610	13570	13380	12720	12310	12020	
10.0	$J_{a,max}$	3.085	3.130	3.174	3.215	3.248	3.286	3.375	3.374	3.451	3.549	3.627	
	$q_{a,max}$	32.82	36.22	38.57	39.84	39.99	39.93	39.30	35.98	31.27	29.70	28.88	
	$T_{a,max}$	11900	12260	12480	12580	12590	12590	12520	12220	11540	11090	10730	

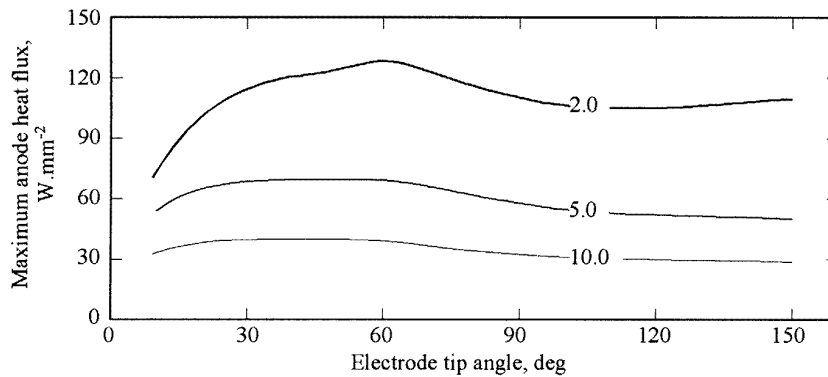


Figure 10. Variation of the maximum anode heat flux with electrode tip angle and arc length. Numbers are arc length in millimetres.

is not constant [32], this condition has practically no effect on the calculation results and it is thus possible to choose a constant temperature, close to the melting point of the electrode material, for the cathode surface.

4.1.2. The anode region. Since the electrical conductivity of the metal is much higher than the plasma, it can be assumed that the electric potential is constant along the anode surface.

For the enthalpy boundary condition, a heat flux from the arc to the anode (workpiece) is considered. Conventionally, the heat flux to the anode can be expressed as [33]:

$$q_a = q_c + q_r + q_e \tag{10}$$

where q_c represents the local heat fluxes by conduction and convection, q_r is the radiation heat transfer and q_e is the energy transferred to the anode by the electrons. The heat transfer by the electrons, q_e , consists of the contribution

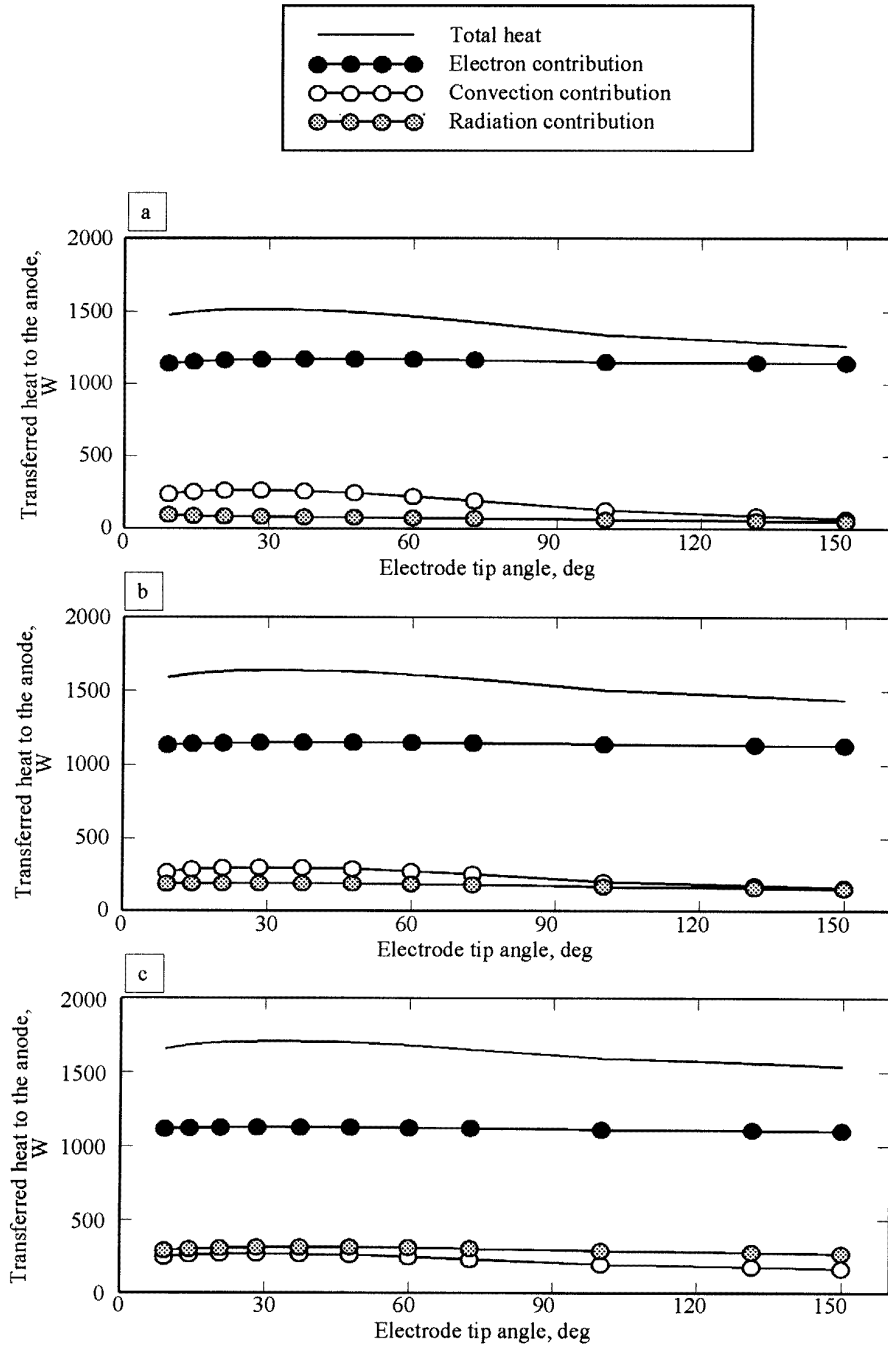


Figure 11. Transferred heat to the anode versus the electrode tip angle for arcs of different lengths. (a) $L_{arc} = 2.0$ mm; (b) $L_{arc} = 5.0$ mm; (c) $L_{arc} = 10.0$ mm.

of the kinetic energy of the electrons, electron flow in the anode sheath layer and electron condensation. Thus the electron contribution can be expressed as follows:

$$q_e = J_a \left(\frac{5}{2} + \frac{e\phi_d}{k_B T_e} \right) \frac{k_B T_e}{e} + J_a \phi_a. \quad (11)$$

By considering an argon plasma with electron temperatures of about 10000 K, the value of the term in parenthesis is 3.203.

To evaluate the convective heat transfer based on the approaches of McKelliget and Szekely [29] and Westhoff [18], the following equation was used:

$$q_c = \frac{0.515}{Pr_w} \left(\frac{\mu_e \rho_e}{\mu_w \rho_w} \right)^{0.11} \left(\mu_w \rho_w \frac{v}{r} \right)^{0.5} (h_e - h_w). \quad (12)$$

The radiation contribution to the anode heat flux can be calculated using the following relationship (figure 4) [18, 29].

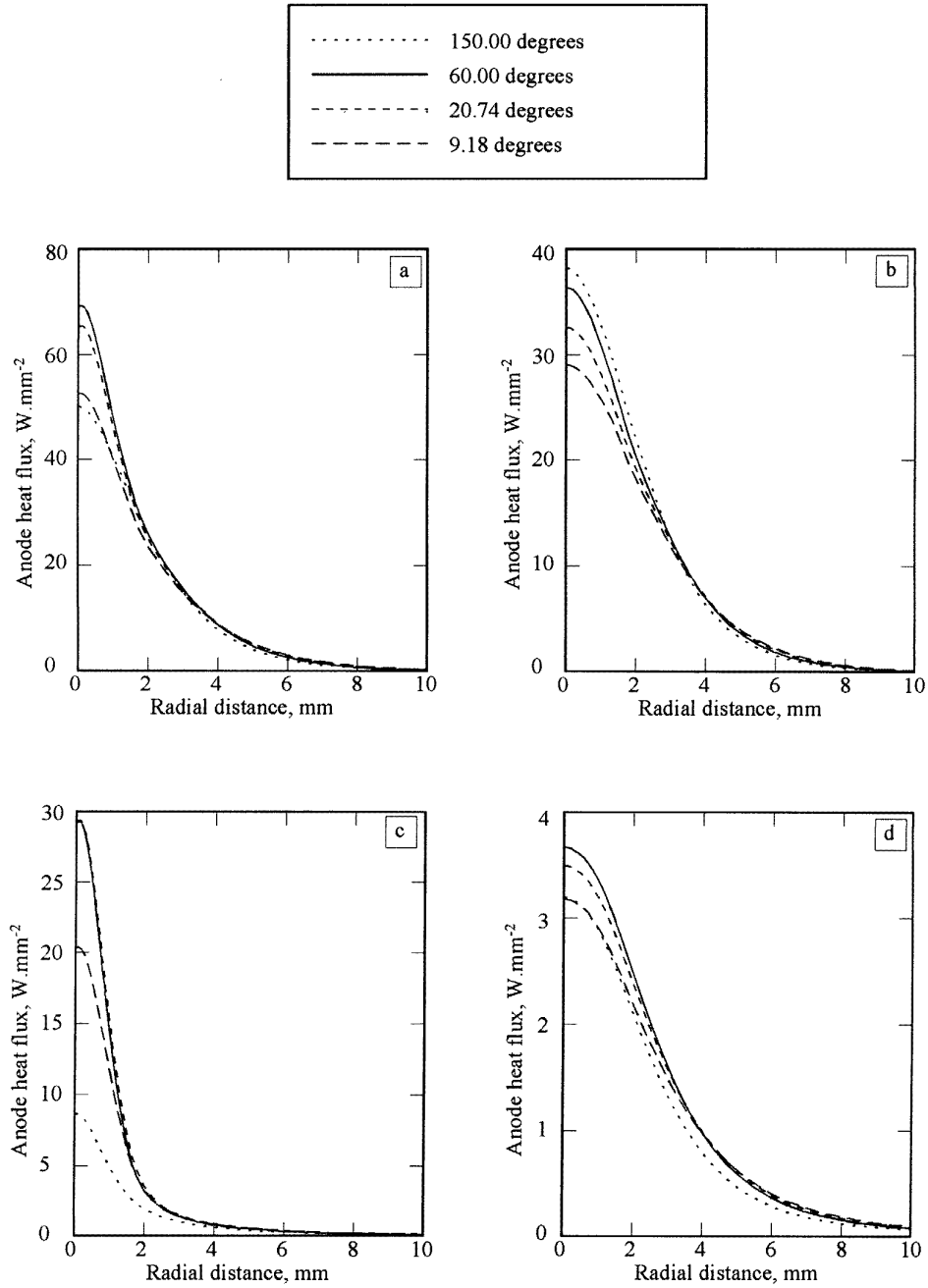


Figure 12. Effect of the electrode tip angle on the radial distribution of the heat flux to the anode. $L_{arc} = 5.0$ mm. (a) Total heat flux; (b) electron contribution; (c) convection contribution; (d) radiation contribution.

$$q_{r,i} = \int_{V_j} \frac{S_{R,j}}{4\pi r_{i,j}^2} \cos \psi \, dV_j. \quad (13)$$

$$\frac{\partial(\rho\Phi)}{\partial t} + \text{div}(\rho v\Phi - \Gamma_\phi \nabla\Phi) = S_\Phi \quad (14)$$

or at steady state

$$\text{div}(\rho v\Phi - \Gamma_\phi \nabla\Phi) = S_\Phi \quad (15)$$

4.2. Numerical method

To solve the above equations, the PHOENICS code was used. This code, developed by Concentration, Heat and Momentum Ltd (CHAM), provides solutions to the discretized version of sets of differential equations having the general form [34]:

where Φ stands for any conserved property, such as enthalpy, momentum and mass. The first term on the left-hand side is the convective term and the second term is the conductive or diffusive term. The term on the right-hand side shows the source rate of Φ . By comparing

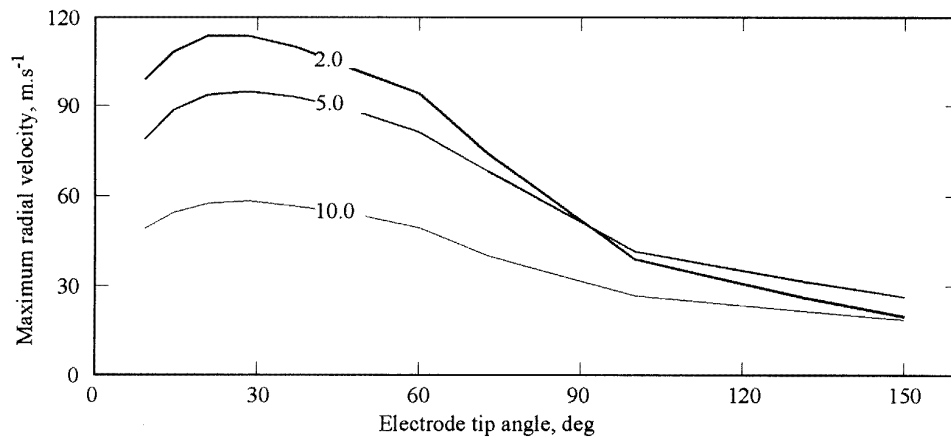


Figure 13. Variation of radial velocity of the gas with the electrode tip angle and arc length. Numbers are arc length in millimetres.

the general form (equation (15)) with the conservation equations (equations (1)–(4)) the associated quantities can be extracted. These quantities are listed in table 2. The continuity of the electric potential can also be solved in this way and it can be treated as a conduction problem without the convection term.

5. Results and discussion

The GTAW model for pure argon was simulated for the range of electrode tip angles of about 10 to 150°. Calculations were also performed for arc lengths of 2.0, 5.0 and 10.0 mm for an applied current of 200 A. The effects of the anode heat flux, anode current density, shear stress and arc pressure on the weld pool due to plasma flow are of primary interest. To verify the results of the proposed model, they will be compared with available experimental results. In the following the effect of the electrode tip angle on the arc properties, especially anode heat flux, anode current density, arc pressure and plasma flow shear stress, will be presented.

5.1. Arc properties

Four major properties of the arc, i.e. maximum temperature, maximum axial velocity, electric potential difference and anode pressure difference for different electrode tip angles and arc lengths are given in table 3.

In figure 5 the temperature profiles of the 10.0 mm arc with 60° electrode tip angle are compared with the results of Hsu *et al* [14]. Although the tip angle for the experimental results is not specified, the agreement between the theoretical and experimental data is excellent even at the cathode boundary. The radial distributions of temperature at 1.5 mm from the tip of the electrode for two different cathode tip angles are compared with the experimental results of Haidar and Farmer [32] in figure 6 where it can be seen that the agreement between the theoretical and the experimental values down to 10 000 K is very good. However, below 10 000 K, the theoretical values decrease sharply. This behaviour is probably due to the absorption of energy, emitted

from the central part of the arc, by the outer part of the arc. Cram *et al* [35] and Farmer and Haddad [36] have shown that at the outer part of the arc, where the temperature is lower than about 10 000 K, the optically thin assumption is not accurate. Therefore it can be concluded that the theoretical temperatures below 10 000 K are not reliable.

Table 3 indicates that the maximum velocity occurred at about a 37° tip angle. This is shown in figure 7 for a 5.0 mm arc. In this figure, the effect of the electrode tip angle on the axial distribution of the axial velocity is illustrated. The maximum velocity is closest to the electrode tip at a 60° angle.

By increasing the arc length from 2.0 to 5.0 mm, the anode pressure remains constant. However, beyond 5.0 mm it decreases (table 3). It was found [37] that decreasing the arc length produces a strong electromagnetic force at the surface of the workpiece towards the axis of symmetry. Therefore, in short arcs there will be a resistance against the gas flow which does not let the pressure at the surface of the workpiece increase.

The arc voltages for different arc lengths for an electrode with a 60° tip angle are compared in figure 8 with the experimental data given in the *Welding Handbook* [2]. The results show a very good agreement. Variation in the arc voltage with the electrode tip angle depends on the mean diameter of the arc and the conductivity of the gas.

5.2. Anode current density and heat flux

The maximum current density, the maximum heat flux and the maximum temperature on the anode surface for different electrode tip angles and arc lengths are summarized in table 4. In most cases, the anode current density increases with the electrode tip angle. It can be concluded that by increasing this angle, the path of the electrons towards the anode becomes more concentrated at the centre part and leads to a higher current density for larger electrode tip angles. Typical variation of the anode current density with the electrode tip angle and the arc length is shown in figure 9. The effect of the electrode tip angle is more significant for short arcs.

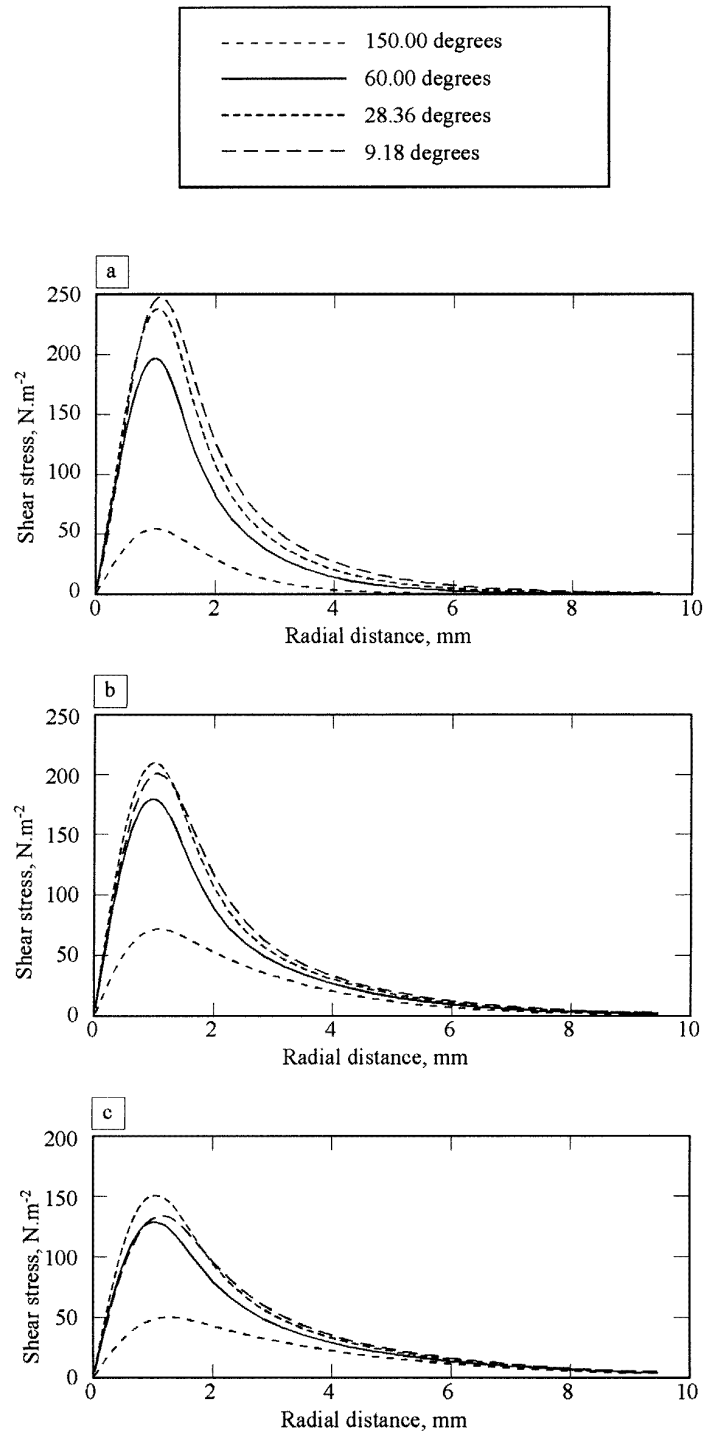


Figure 14. Effect of the electrode tip angle on the distribution of shear stress in arcs with different lengths. (a) $L_{arc} = 2.0$ mm; (b) $L_{arc} = 5.0$ mm; (c) $L_{arc} = 10.0$ mm.

The effect of the electrode tip angle and arc length on the maximum heat flux to the anode is shown in figure 10. The maximum heat flux to the anode occurred between 30 and 60°. The same behaviour was observed in the total heat transferred to the anode. Variation of the total heat and also the contributions of the three different mechanisms with the electrode tip angle and arc length is shown in figure 11. It is

obvious that the electron heat flux is the major mechanism of heat transfer to the anode. The absolute value of heat due to electrons remains almost constant with change in the angle of the electrode tip, but its contribution to the total heat decreases with increasing arc length.

Convective heat transfer is the most sensitive mechanism to the electrode tip angle. The variation in

convection causes the variation in the total heat. The radiation and electron heat transfer mechanisms do not show significant change with the electrode tip angle. On the other hand, the variation in the radiation heat transfer with arc length is the most significant. For long arcs, the contribution of radiation is more than that of convection (figure 11).

The effect of the electrode tip angle on the distribution of the total heat flux and the three heat transfer mechanisms for the 5.0 mm arc are shown in figure 12. The most significant change is related to convection. By decreasing the angle from 150° to about 38° (which is not shown in this graph), the maximum heat flux due to convection increases about four times. The heat flux due to convection spreads over a very small area at the central part of the anode, while the two other mechanisms are spread over a large area.

5.3. Shear stress

To evaluate the shear stress, Westhoff's [18] approach was used. The shear stress acting on the surface can be calculated by the following equation:

$$\tau = \mu(\partial v/\partial z). \quad (16)$$

The effects of the electrode tip angle and the arc length on the maximum radial velocity at the anode surface are illustrated in figure 13. The effect of the tip angle is the most significant for the shortest arc. Figure 13 shows that for the sharp electrode, the maximum radial velocity for the 2.0 mm arc is the highest but by increasing the tip angle it decreases to about the maximum radial velocity for the 10.0 mm arc.

The effects of the electrode tip angle and arc length on the distribution of the shear stress at the anode surface are shown in figure 14. As illustrated, a sharp electrode can increase the shear stress by 2.5 to more than four times. For the 2.0 mm arc, although the maximum radial velocity for the 28.36° electrode tip is the highest (figure 13), the shear stress in the case of the 9.18° tip is higher than that of the 28.36° tip. This is due to the difference in gas temperature and hence in gas viscosity.

6. Conclusion

Applying a variable cathode surface area with the electrode tip angle resulted in a very good agreement of the calculated results with the experimental data, for a wide range of the electrode tip angles from 10° to about 150° for temperatures higher than 10 000 K.

Increasing the tip angle led to shrinkage in the arc diameter. Therefore the anode current density and the heat flux due to the electrons increased with the tip angle. On the other hand, decreasing the electrode tip angle increased the gas velocity and therefore the convective contribution to the anode heat flux. The highest heat flux occurred for electrode tip angles in the range of 30 to 60°.

Decreasing the electrode tip angle from 150 to 10° caused the pressure on the surface of the anode to increase by two to more than three times, depending on the arc

length. The maximum pressure at the anode surface occurred at angles of 20–30°. The shear stress increased significantly with decrease in the electrode tip angle. Increases in both the pressure and the shear stress with the arc length were considerable. Thus, the surface of the weld pool tends to be more unstable with shorter arcs due to the high pressure and the high shear stress. This suggests that, for shorter arcs, it is better to use an electrode with wider tip angles to obtain a smoother welding surface.

Acknowledgments

One of the authors (MG) acknowledges and appreciates a Scholarship from The Ministry of Culture and Higher Education of IR of Iran. The authors are also grateful to the Canadian Natural Science and Engineering Research Council for financial support of this project.

References

- [1] Zacharia T I and David S A 1993 Heat and fluid flow in welding *Mathematical Modelling of Weld Phenomena* ed H Cerjak and K E Easterling (London: Institute of Materials) pp 3–23
- [2] 1991 *Welding Handbook* vol 2, ed R L O'Brien, 8th edn (American Welding Society)
- [3] Kou S and Wang Y H 1986 Weld pool convection and its effects *Welding J.* **65** 63s–70s
- [4] Oreper G M and Szekely J 1984 Heat and fluid flow phenomena in weld pools *J. Fluid Mech.* **147** 53–79
- [5] Kou S and Sun D K 1985 Fluid flow and weld penetration in stationary arc welds *Metall. Trans. A* **16A** 203–13
- [6] Choo R T C and Szekely J 1990 The effect of gas shear stress on Marangoni flows in arc welding *Welding J.* **69** 223s–33s
- [7] Glickstein S S and Friedman E 1984 Weld modelling applications *Welding J.* **63** 38–42
- [8] Saedi H R and Unkel W 1989 Thermal-fluid model for weld pool geometry dynamics *J. Dynam. Syst. Meas. Control* **111** 268–76
- [9] Zacharia T, Eraslan A H, Aidun D K and David S A 1989 Three-dimensional transient model for arc welding process *Metall. Trans. B* **20B** 645–59
- [10] Bertram L A and Kanouff M P 1991 A proposed standard problem definition for the calculation of heat and fluid flow in a GTA weld pool *Modelling of Casting, Welding and Advanced Solidification Processes (Warrendale, PA)* vol V, ed M Rappaz *et al* (Minerals, Metals & Materials Society) pp 733–41
- [11] Correa S M and Sundell R E 1986 A computational and experimental study of the fluid flow in weld pools *Modelling and Control of Casting and Welding Processes (Warrendale, PA)* vol III, ed S Kou and R Mehrabian (TMS-AIME) pp 211–27
- [12] Kim S D and Na S J 1989 A study on heat and mass flow in stationary gas tungsten arc welding using numerical mapping method *Proc. Inst. Mech. Eng. Part B: J. Eng. Manufac.* **203** B4 233–42
- [13] Lee P D 1989 *MASc Thesis* Department of Metallurgy and Materials Science, University of Toronto
- [14] Hsu K C, Etemadi K and Pfender E 1983 Study of free-burning high-intensity argon arc *J. Appl. Phys.* **54** 1293–301

- [15] Hsu K C and Pfender E 1983 Two-temperature modelling of the free-burning high-intensity arc *J. Appl. Phys.* **54** 4359–66
- [16] Kovitya P and Lowke J J 1985 Two-dimensional analysis of free-burning arcs in argon *J. Phys. D: Appl. Phys.* **18** 53–70
- [17] Kovitya P and Cram L E 1986 A two-dimensional model of gas tungsten welding arcs *Welding J.* **65** 34–9
- [18] Westhoff R C 1989 *SM Thesis* Department of Materials Science and Engineering, The Massachusetts Institute of Technology
- [19] Tsai M C and Kou S 1990 Heat transfer and fluid flow in welding arcs produced by sharpened and flat electrodes *Int. J. Heat Mass Transfer* **33** 2089–98
- [20] Delalondre C and Simonin O 1990 Modelling of high intensity arcs including a non-equilibrium description of the cathode sheath *J. Physique Coll.* **51** C5 18 199–206
- [21] Jog M A, Cohen I M and Ayyaswamy P S 1991 Heat transfer in electric arc welding *Welding and Joining Processes (New York)* ed E Kannatey-Asibu Jr *et al* (American Society of Mechanical Engineers) **PED-51** 135–42
- [22] Zhu P, Lowke J J and Morrow R 1992 A unified theory of free-burning arcs; cathode sheaths and cathodes *J. Phys. D: Appl. Phys.* **25** 1221–30
- [23] Lowke J J, Kovitya P and Schmidt H P 1992 Theory of free-burning arc columns including the influence of the cathode *J. Phys. D: Appl. Phys.* **25** 1600–6
- [24] Lowke J J, Zhu P, Morrow R, Haider J and Farmer A J D 1993 Onset of cathode and anode melting by electric arcs *Proc. 11th Int. Symp. Plasma Chem. (Loughborough, UK, 1993)* ed J E Harry, pp 245–50
- [25] Zhu P, Lowke J J, Morrow R and Haider J 1995 Prediction of anode temperature of free burning arcs *J. Phys. D: Appl. Phys.* **28** 1369–76
- [26] Kaddani A, Zahrai S, Delalondre C and Simonin O 1995 Three-dimensional modelling of unsteady high-pressure arcs in argon *J. Phys. D: Appl. Phys.* **28** 2294–305
- [27] Pfender E 1978 Electric arcs and arc gas heaters *Gaseous Electronics* vol 1, ed M N Hirsh and H J Oskam (New York: Academic) pp 291–398
- [28] Mitchener M and Kruger C H Jr 1992 *Partially Ionized Gases* (New York: Wiley)
- [29] McKelliget J and Szekely J 1986 Heat transfer and fluid flow in the welding arc *Metall. Trans. A* **17A** 1139–48
- [30] Boulos M I, Fauchais P and Pfender E 1994 *Thermal Plasma, Fundamentals and Applications* vol 1 (New York: Plenum)
- [31] Evans D L and Tankin R S 1967 Measurement of emission and absorption of radiation by an argon plasma *Phys. Fluids* **10** 1137–44
- [32] Haider J and Farmer A J D 1994 Large effect of cathode shape on plasma temperature in high-current free-burning arcs *J. Phys. D: Appl. Phys.* **27** 555–60
- [33] Pfender E 1980 Energy transport in thermal plasmas *Pure Appl. Chem.* **52** 1773–800
- [34] CHAM *TR100—A Guide to the PHOENICS Input Language*
- [35] Cram L E, Poladian L and Roumeliotis G 1988 Departure from equilibrium in a free-burning argon arc *J. Phys. D: Appl. Phys.* **21** 418–25
- [36] Farmer A J D and Haddad G N 1988 Rayleigh scattering measurements in a free-burning argon arc *J. Phys. D: Appl. Phys.* **21** 426–31
- [37] Goodarzi M 1997 *PhD Thesis* Department of Metallurgy and Materials Science, University of Toronto